

Cooperative AUV Navigation using a Single Maneuvering Surface Craft

Maurice F. Fallon, Georgios Papadopoulos, John J. Leonard and Nicholas M. Patrikalakis

Abstract

This paper describes the experimental implementation of an online algorithm for cooperative localization of submerged autonomous underwater vehicles (AUVs) supported by an autonomous surface craft. Maintaining accurate localization of an AUV is difficult because electronic signals, such as GPS, are highly attenuated by water. The usual solution to the problem is to utilize expensive navigation sensors to slow the rate of dead-reckoning divergence. We investigate an alternative approach that utilizes the position information of a surface vehicle to bound the error and uncertainty of the on-board position estimates of a low-cost AUV. This approach uses the Woods Hole Oceanographic Institution (WHOI) acoustic modem to exchange vehicle location estimates while simultaneously estimating inter-vehicle range. A study of the system observability is presented so as to motivate both the choice of filtering approach and surface vehicle path planning. The first contribution of this paper is the presentation of an experiment in which an extended Kalman filter (EKF) implementation of the concept ran online on-board an OceanServer Iver2 AUV while supported by an autonomous surface vehicle moving adaptively. The second contribution of this paper is provide a quantitative performance comparison of three estimators: particle filtering (PF), Nonlinear Least Squares optimization (NLS), and the EKF for a mission using three autonomous surface craft (two operating in the AUV role). Our results indicate that the PF and NLS estimators outperform the EKF, with NLS providing the best performance.

I. INTRODUCTION

Improved navigation of multiple vehicles is essential to improve the accuracy and efficiency of many AUV missions, such as mine-hunting, disaster response, and oceanographic surveys.

The Authors are with the Computer Science and Artificial Intelligence Laboratory, Massachusetts Institute of Technology, Cambridge, MA 02139, USA. Email: mfallon, gpapado, jleonard, nmp@mit.edu

Tracking examples can be viewed at <http://people.csail.mit.edu/mfallon>

This paper provides an experimental investigation of techniques for cooperative localization of multiple AUVs, using a single surface vehicle to aid the navigation of submerged vehicles. This work generalizes the moving long baseline (MLBL) navigation approach originally proposed by Vaganay *et al.*[36] and Bahr and Leonard [4], relaxing the requirement to have two vehicles serving as communication navigation aids (CNAs). The vehicles used in our experiments are shown in Figure 1.

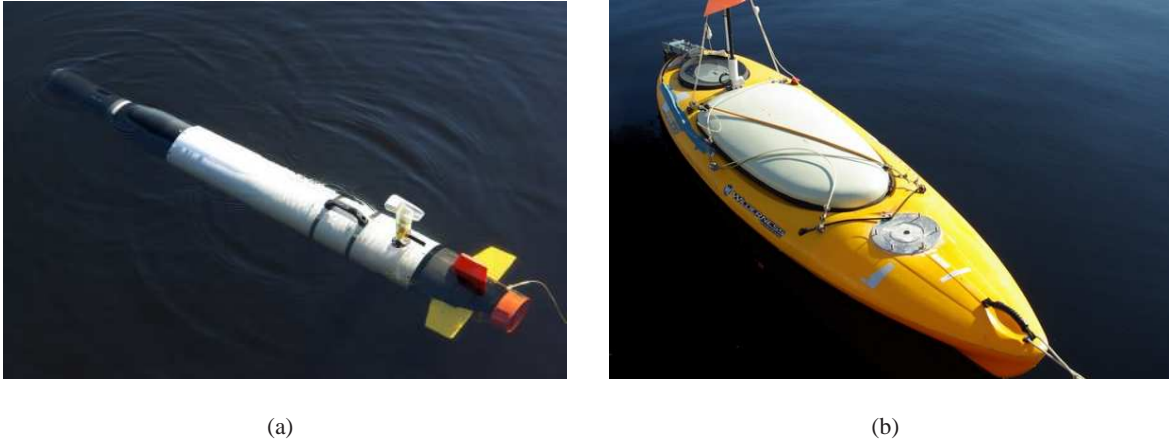


Fig. 1. The vehicles used in our experiments: (a) the OceanServer Iver2 AUV; (b) the MIT Scout kayak which functioned as the CNA.

AUV navigation is a difficult problem that has been the subject of a large amount of research in the past several decades [39]. The technologies available for providing localization information to an AUV include: (1) dead reckoning using proprioceptive sensing, (2) surfacing for GPS fixes, and (3) acoustic beacon systems. Proprioceptive navigation refers to using measurements of the vehicle's self-motion to deduce the vehicle's position. There are two major categories, based on price: (a) inertial navigation systems (INS) combined with Doppler velocity log (DVL) sonars and (b) magnetic compass/attitude heading reference systems. Regardless of sensor cost and quality, the problem with exclusive reliance on proprioceptive sensing is that position error increases without bound as the distance traveled by the vehicle increases. The rate of increase will be a function of ocean currents, the vehicle speed, and the quality of dead reckoning sensors. If a vehicle can surface, then GPS can be used for a position fix. Indeed, many AUVs have demonstrated this capability [30], [23], [1]. However, frequent surfacing is impractical for deep-water missions and is undesirable for many other AUV missions of interest.

In acoustic navigation, transponders serve as beacons to constrain INS/DR error growth without the need for resurfacing. Two types of systems have been primarily employed [15], [17], [25]: long baseline (LBL) and ultra-short baseline (USBL). Both systems employ external transducers or transducer arrays as aids to navigation. Acoustic navigation of AUVs is a well-established technique that has been widely used on many different types of AUVs [35], [39], [33], [40]. The use of static beacons restricts the area of operations to a few km^2 , making some missions of interest impractical with this approach.

The desire to extend acoustic navigation to a wider area of operation motivates a system in which multiple vehicles can use one another as “mobile beacons”. The majority of modern AUVs already have an acoustic modem for command and control; using ranges derived from it we aim to achieve geo-referenced navigation without adding additional sensors to the vehicles. Acoustic modems are available from a few thousand dollars and are orders of magnitude cheaper than low-end DVL or INS units. Our approach instead utilizes a dedicated surface vehicle (with access to GPS) communicating with a fleet of AUVs so as to improve the positioning of the latter. The main contribution presented in this paper is to use only a single CNA vehicle, instead of two as in previous work [36], [4]. Our results include the first (to our knowledge) online navigation of a submerged AUV using acoustic range measurements transmitted from a single autonomous surface vehicle. Using only a single surface vehicle has a significant effect on both the filtering approach used by the AUV and the required mobility of the surface vehicle. We also present a detailed comparison between the EKF, particle filter, and nonlinear least squares estimators, which illustrates that the latter gives superior performance and should be used going forward for this application.

A number of previous researchers have performed experiments involving an AUV obtaining range measurements to a single transponder. Larsen developed an approach termed Synthetic LBL [22], which used measurements from a single acoustic transponder at an unknown location to constrain the error growth of a high performance INS system [21]. LaPointe developed techniques for using range measurements from a single transponder for deep sea positioning, extending the operating area beyond that of a typical LBL transponder network [20]. Vaganay *et al.* investigated techniques for homing to an acoustic beacon using only range measurements [34]. Stilwell and colleagues [24], [14], [13] have implemented a system in which an AUV can localize itself by using a single ranging beacon at known position while also measuring the water current.

Webster, Eustice and colleagues [10], [37], [38] have utilized a single research ship to support an underwater vehicle navigating using the WHOI acoustic modem; their approach is closely related to the approach presented in this paper. Rigby *et al.* [31] studied the fusion of USBL and DVL sensors to form a more accurate geo-referenced navigation system with bounded error underwater which could be mobile beyond a fixed location. In both the Webster *et al.* and Rigby *et al.* research, the AUV's proprioceptive sensors were significantly more precise than the vehicles used for our experiments; in addition, the surface vehicle did not maneuver autonomously and only one AUV was considered.

Multiple AUV navigation falls within the broader problem of multi-robot cooperative localization which has been studied in great depth by Roumeliotis and colleagues. Mourikis *et al.* [26] provides a performance analysis of the cooperative localization problem. More recently, Nerurkar *et al.* [27] proposed a Distributed Conjugate Gradient (DCG) *maximum a posteriori* algorithm for distributed localization of a group of vehicles, developing efficient methods to limit the communication cost and computational complexity for large multi-robot teams (with simulation results presented for a team of 18 robots). Our work targets the underwater environment, where severe communications constraints would make such an approach difficult to implement.

Meanwhile Djugash *et al.* [6], [8], [7] have studied localization with range-only measurements from stationary radio beacons. Their work has considered issues such as localization of a moving indoor robot given poor dead-reckoning or measurement dropouts, as well as simultaneous estimation of the beacon location — a variant of SLAM. Their work has also used a polar coordinate system, rather than Cartesian, so as to more accurately represent the vehicle probability distributions.

In this paper, we outline the extension of the MLBL concept to using only one surface vehicle aiding the navigation of one or more AUVs by providing georeferenced range measurements. Utilizing a single surface vehicle requires concurrent operation of surface vehicle motion planning and filtering algorithms which requires consideration of system observability so as to maintain stable and scalable performance. Each of these issues are discussed in this paper. The first experimental contribution of this paper is the presentation of an experiment in which an EKF-based implementation of the approach ran online on-board an OceanServer Iver2 AUV while supported by an autonomous surface vehicle moving adaptively. The second experimental contribution of this paper is to provide a quantitative performance comparison of

three estimators: particle filtering (PF), Nonlinear Least Squares optimization (NLS), and the EKF for a mission using three autonomous surface craft (two operating in the AUV role).

In Section II the limitations and assumptions of this basic approach are discussed. Our algorithm is outlined in Section III as well as some analysis which illustrates the importance of surface vehicle motion planning. Suitable motion planning behaviors are also discussed. Section IV introduces three online filtering and smoothing algorithms which have been considered for this application - the Extended Kalman Filter (EKF), the Particle Filter and Nonlinear Least Squares (NLS) and discusses the merits of each.

Section V presents the results of several experiments which illustrate our proposed concept including an online EKF-based experiment with an OceanServer Iver2 AUV. A detailed comparison between the three filtering and smoothing algorithms is then presented. Finally, conclusions drawn from these experiments and directions of future work are discussed in Section VI.

II. UNDERWATER COOPERATIVE LOCALIZATION

While maintaining the core concept introduced in [4], we will instead assume there to be only one surface vehicle providing the submerged fleet of AUVs with its GPS-derived position information. This vehicle may also be operating as a communications moderator — in the dual role of a Communications and Navigation Aid (CNA, see Figure 1). Meanwhile each autonomous underwater vehicle will maintain a dead reckoning filter, drawing upon measurements of velocity, heading and depth.

Communication between the vehicles is possible using the WHOI acoustic modem [12]. In our experiments, this system provides transmission rates of the order of 32 bytes per 10 seconds. Transmission of a packet consists of two stages: first a *mini packet* is transmitted to initiate the communication sequence. The time-of-flight, t_k , and hence the inter-vehicle range can be estimated using this mini packet using the speed of sound in water, $z_{3D,k} = c \times t_k$. Following this, the information packet is transmitted in a process which lasts approximately 5-6 seconds. In all, it is prudent to reserve 10 seconds per transmission.

Time-of-flight is calculated using a precisely synchronized on-board pulse-per-second (PPS) timing board, as detailed in [10]. The PPS is maintained using a COTS low-power temperature compensated crystal oscillator combined with a micro-controller PCB (for higher-level functionality). Experiments by the authors suggested a maximum drift-induced range bias of 0.45m over

24 hours.

As the depth of the AUV can be easily and precisely instrumented, the 3D range estimate will be transformed into a 2D planar range at the outset and all references to range in what follows will concern this 2D planar range,

$$z_k = \sqrt{z_{3D,k}^2 - (d_C - d_A)^2} \quad (1)$$

where the depth of the CNA and AUV are given by d_C and d_A respectively.

The packet transmitted from the CNA shall contain its position ($X_{C,k}$), depth and heading as well as a UNIX time-stamp. The uncertainty of the CNA's position estimate is not included in the packet because when operating in the open ocean this value will be static and known to the AUV in advance. Similarly the AUV will transmit a message containing its own position estimate and associated covariance which can be used to help the CNA plan its own supporting motion — also requiring 10 seconds per transmission. See Section III-B for more discussion regarding motion planning.

Round Trip Ranging: In terms of scalability, one-way-ranging allows any number of AUVs within the broadcast range of the CNA to estimate range and to receive the CNA transmissions. However an alternative feature of the WHOI modem is round-trip ranging for use with modems without access to accurate time synchronization. One vehicle's modem (in our setup the CNA) transmits a mini-packet (or *ping*) to a specific modem id. The receiving vehicle receives it and replies after a small, known time. The CNA then receives the reply and measures the elapsed time and calculates the range using the speed of sound in water. While the elapsed time can be accurately measured; the range estimate will be less accurate than the one way range estimates due to the relative movement of the vehicles during transmission. Having measured the round-trip range, the value will be transmitted back to the AUV with the corresponding CNA position in a regular 32 byte pack.

Unlike with the one way range system, this position will be at least 10 seconds old (the full packet transmission time) when received by the AUV. For this reason it is necessary to buffer the AUV inertial measurements for this period and to correct the AUV's corresponding historical position estimate before integrating the buffer of AUV inertial measurements up to the current time (see Figure 2).

While this approach does not require a precisely synchronized clock, it does require ranging

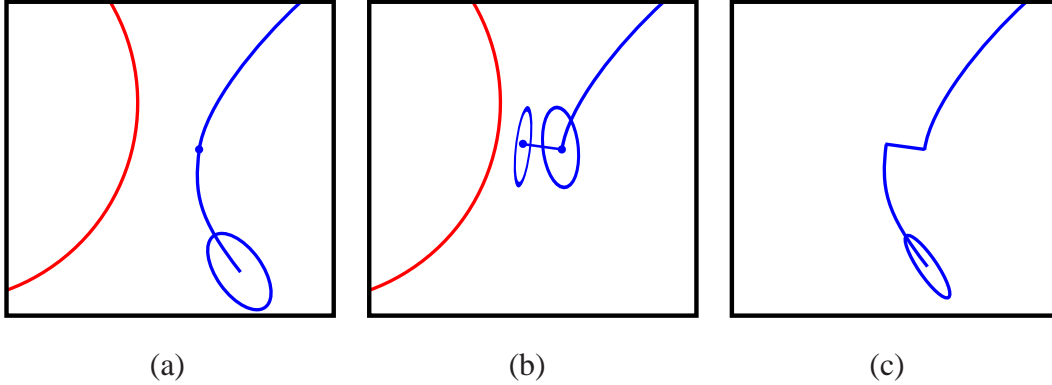


Fig. 2. Using the Round Trip Ranging mode the filter operates out of sequence. (a) First a round trip range measurement is received from the CNA (as illustrated in red) which corresponds to a previous AUV position (the blue dot) rather than the current position. (b) Using a buffer of dead-reckoning measurements the filter position and covariance matrix are reset to the corresponding values and the usual position optimization is carried out. (c) Finally the buffered dead-reckoning is reapplied, giving the AUV a better estimate of its position.

of each vehicle individually which is not a satisfactory scaling (for the same reasons as the USBL approach in [31]). Nonetheless, the feature has been implemented as part of our software implementation as a fallback solution. Experiment 1B in Section V illustrates that performance is not significantly worse than one way ranging.

III. SINGLE SURFACE CRAFT COOPERATIVE NAVIGATION

Consider a single CNA supporting N underwater vehicles. Each AUV will maintain an estimate of its own position, $X_{A,k} = [x_{A,k}, y_{A,k}, \theta_{A,k}]$, and an associated covariance matrix. This estimate will be regularly propagated (typically at 10Hz) so as to integrate heading ($\hat{\theta}_k$), forward (\hat{v}_k) and starboard velocity (\hat{w}_k) measurements. Neglecting the vehicle id for now; at time k the propagation equations will be

$$\begin{aligned}
 x_k &= x_{k-1} + \Delta_k(\hat{v}_k \cos \hat{\theta}_k + \hat{w}_k \sin \hat{\theta}_k) \\
 y_k &= y_{k-1} + \Delta_k(\hat{v}_k \sin \hat{\theta}_k - \hat{w}_k \cos \hat{\theta}_k) \\
 \theta_k &= \hat{\theta}_k
 \end{aligned} \tag{2}$$

This dead-reckoning estimate will be combined with the CNA range and position information using a filtering or smoothing algorithm to produce a corrected position estimate with reduced

and eventually bounded uncertainty. Three such algorithms will be discussed in Section IV.

Before discussing the algorithms specifically, it is necessary to consider how measurement observability effects AUV estimation.

A. Observability Analysis

It is envisaged that MLBL will be integrated within a multi-AUV setup in which use of the communication channel will be shared. As a result the transmission rate of a position/range pair is likely to be substantially below one measurement per 10 seconds. Furthermore only a portion of transmitted messages will actually be received. For these reasons it is prudent to maximize the benefit achieved from integrating CNA range measurements by planning CNA motion trajectories which best contribute to AUV localization. This requires examination of the observability of the AUV given the CNA measurements and the relative positions of the two vehicles.

We will first determine the conditions by which the proposed linearized system and the actual non-linear system are observable. Linearizing the actual non-linear system, Gadre *et al.* [13], [14] have proven that a vehicle which consistently observes its range to a beacon located at the same relative direction is locally unobservable (although presented in the less general case of a stationary range beacon). A path of this type of motion is illustrated in Figure 3(a). Alternatively, if the relative positions of the vehicles is varied, as shown in Figure 3(b) and Figure 3(c), system observability can be obtained when using a linearized filter, such as an EKF. Since the AUV mission is usually predetermined, it falls on the CNA to plan an intelligent path to achieve this.

Secondly, for a nonlinear estimator, such as a particle filter or nonlinear least square optimization (NLS), of a non-linear measurement function, h , can observe the system if the gradient of the Lie derivative matrix, G , is a full rank matrix, according to the weak observability theorem [32], [16]. The observability matrix is given by

$$Obs = d(G) = \begin{pmatrix} dL_f^0(h_1) & \dots & dL_f^0(h_m) \\ dL_f^1(h_1) & \dots & dL_f^1(h_m) \\ \vdots & \ddots & \vdots \\ dL_f^{n-1}(h_1) & \dots & dL_f^{n-1}(h_m) \end{pmatrix} \quad (3)$$

where $L_f^{n-1}(h_m)$ is the Lie derivative of the measurement m in dimension n .

While our dynamical system, Equation 2, is a third order system, we have access to a direct estimate of the heading. For this reason we can simplify the observability analysis to a second

order system in x and y , thus $n = 2$. The continuous system equivalent is given by

$$\dot{X}_A = f(X_A, u) \quad (4)$$

where

$$f = \begin{pmatrix} f_1 \\ f_2 \end{pmatrix} = \begin{pmatrix} \hat{v} \cos \hat{\theta} + \hat{w} \sin \hat{\theta} \\ \hat{v} \sin \hat{\theta} - \hat{w} \cos \hat{\theta} \end{pmatrix} \quad (5)$$

For the range-only measurements, with $m = 1$, the non-linear measurement function is given by

$$h = h_1 = \sqrt{(X_A - X_C)^T (X_A - X_C)} = \sqrt{(x_A - x_C)^2 + (y_A - y_C)^2} \quad (6)$$

the Lie derivatives are as follows

$$L_f^0(h) = h \quad (7)$$

$$L_f^1(h) = \begin{pmatrix} \frac{x_A - x_C}{h} & \frac{y_A - y_C}{h} \end{pmatrix} \begin{pmatrix} f_1 \\ f_2 \end{pmatrix} \quad (8)$$

which gives

$$G = \begin{pmatrix} h \\ \frac{(x_A - x_C)f_1 + (y_A - y_C)f_2}{h} \end{pmatrix} \quad (9)$$

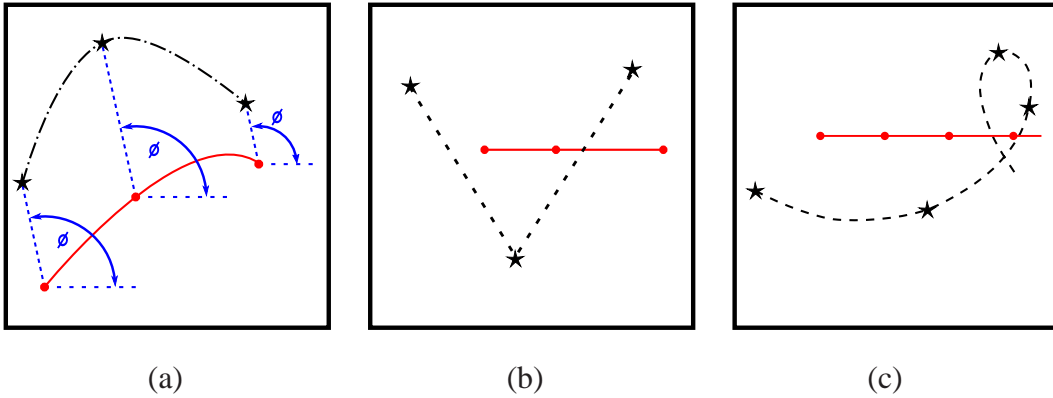


Fig. 3. Observability: Should the AUV (red line) receive range measurements from the CNA (black dashed line) from the same relative direction, ϕ , then the linearized system will be unobservable, but the actual non-linear system will be observable (a). Should the CNA maneuver to achieve radial coverage by zig-zagging (b) or encircling the AUV (c), then the CNA path can be fully observed. These two motion plans are demonstrated experimentally in Section V. Each marker represents the respective vehicle locations during a measurement/transmission.

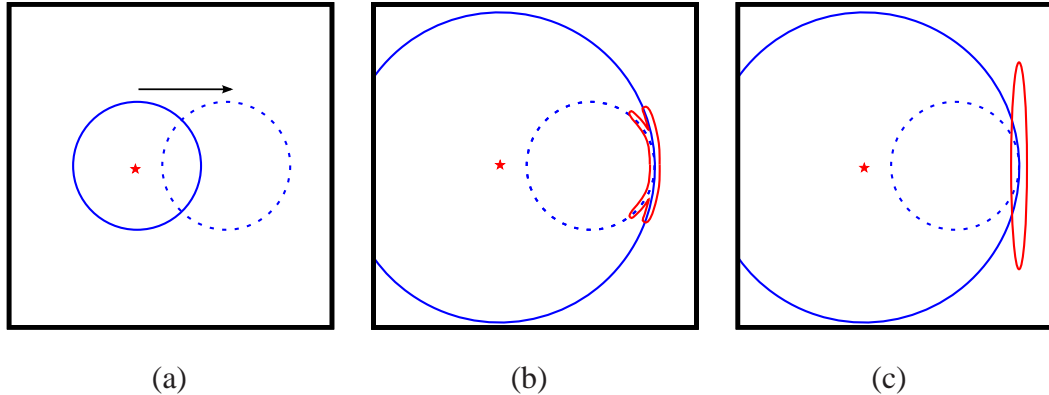


Fig. 4. Despite moving directly away from a stationary CNA, an AUV can remain observable using a non-linear estimator. (a) Having received a range measurement from a static CNA (positioned at the red star), the AUV (at an unknown position) moves relatively as indicated by the black arrow and translated range circle. (b) If another range measurement is received from the CNA, a (non-linear) particle filter could estimate the position of the AUV (as indicated by the non-parametric distribution in red). (c) Meanwhile an EKF would badly represent the received information and would typically diverge.

Our specific observability matrix is formed from the gradient of G with respect to the AUV state vector X_A

$$Obs = d(G) = d \begin{pmatrix} L_f^0(h) \\ L_f^1(h) \end{pmatrix} \quad (10)$$

$$= \begin{pmatrix} \frac{(x_A - x_C)}{h} & \frac{(y_A - y_C)}{h} \\ \frac{(y_A - y_C)^2 f_1 - (x_A - x_C)(y_A - y_C) f_2}{h^3} & \frac{-(x_A - x_C)(y_A - y_C) f_1 + (x_A - x_C)^2 f_2}{h^3} \end{pmatrix} \quad (11)$$

This system is observable if the observability matrix is full rank. Thus, if

$$\det(Obs) = \frac{-f_1(y_A - y_C) + f_2(x_A - x_C)}{h^2} \neq 0 \quad (12)$$

Except for some trivial special cases, the system identified as being unobservable for linearized systems, [13], is now observable for nonlinear systems, as long as the CNA-AUV range changes. This is illustrated graphically in Figure 4. Nonetheless, if the relative positions of the vehicles are not varied, the uncertainty in the axis perpendicular to the CNA-AUV axis will remain large — even with successive ranging steps — which again motivates intelligent CNA motion planning.

In summary, the observability of the linearized system is provided by the relative motion between the vehicles, but can be improved upon by the using the actual nonlinear system as

well as CNA motion planning.

B. Surface Craft Path Planning

Within the constraints of its command and control functions, the CNA will plan a path so as to transmit from the locations which best allow the AUVs to reduce their uncertainties. How this path should be planned depends upon how dedicated the communication system is to the task of cooperative localization as well as the mobility of the CNA when compared to the AUV fleet. Consider three scenarios:

- Transmission only when a sufficient uncertainty reduction can be accrued.
- Maintenance of a certain upper bound on the vehicle uncertainty.
- Complete or significant usage of the communication channel.

The first scenario considers the role of MLBL as part of a wider experimental system and would require a mission dependent solution. See [2] for a more complete discussion of this scenario. The second scenario is more general, and in this case the relative velocities of the vehicles would be an important limiting factor.

The final scenario is the most basic operational scenario and has been explored in the experiments in Section V for the two different motion behaviors illustrated in Figure 3(b) and (c). It should be noted that uncertain path planning is part of a more general field of research and is not fully examined in this publication. In related work on this topic in the context of MLBL, Bahr and Leonard [3] investigated motion strategies for the CNA to minimize trilateration errors.

We have implemented two conservative greedy algorithms in Section V which illustrate the concept. One maintains a 45 degree zig-zagging pattern behind the AUV while the other encircles the AUV continuously. Both keep a significant standoff distance — calculated using the AUV position estimate and uncertainty — so as to avoid baseline ambiguity. In each case the CNA chooses a new waypoint based on the AUV's current position estimate and uncertainty. During transit it will communicate with the AUV several times, updating its knowledge of the AUV's status. Upon reaching the waypoint, a new waypoint will again be determined using the AUV position estimate.

IV. MEASUREMENT FILTERING AND OPTIMIZATION

Thus far we have not specifically discussed the fusion of the proprioceptive and exteroceptive measurements. Our earlier work, [4], proposed an algorithm which utilized the on-board dead reckoning estimate of the AUV and a pair of CNA range estimates to produce a complete estimate of the AUV state vector as well as a measure of confidence. Having collated these measures for all such pairs of estimates, a best estimate of the position was proposed. This approach was predicated upon an assumption that the range measurement distribution was multi-modal.

The seabed, the water surface and deep sea thermoclines within the water body have the ability to cause significant multi-path signal interference and the receipt of a substantial amount of infeasible outlier measurements. A typical Long Baseline ranging data set is illustrated in Olson *et al.* [29], illustrating the potential difficulty in processing LBL data. However the advanced processing within the WHOI modem decoder has the ability to suppress the bulk of these effects, such that the received range measurements decoded by the modem contain only a moderate amount of noise, as shown in Figure 5. The distribution is experimentally studied in Section V-A.

Instead we will consider three filtering and smoothing techniques in this paper:

- Extended Kalman Filter
- Particle Filter
- Nonlinear Least Squares Optimization.

Initially an **Extended Kalman Filter** (EKF) was implemented on-board our vehicle fleet. Both imprecise CNA GPS position estimates and biased or nonlinear AUV actuation measurements have been observed to lead to unpredictable corrections to the EKF position estimate. These erroneous corrections require a significant period of time before re-convergence to the true estimate. Nonetheless, this approach have been tested online due to its simplicity and is presented in Section V-B.

Its prediction step is as in Equation 2 while the measurement residual equation is as follows

$$y_k = z_k - \mathbf{H}_k \|\hat{\mathbf{X}}_{A,k} - \hat{\mathbf{X}}_{C,k}\| \quad (13)$$

where z_k is the range measurement and \mathbf{H}_k the Jacobian measurement matrix.

Particle Filtering is an alternative recursive state estimator which uses a sample-based approach to represent a probability distribution. It has the ability to capture both nonlinearity in

the motion model and non-Gaussianity in the measurement function [9]. In particular we are interested in its ability to properly represent the ambiguity during baseline crossings and to facilitate uncertain vehicle initializations (Section V-D). Particle filters also have the ability to function successfully when sensors measurements are biased or known to be poorly calibrated, as recognized by [31].

In Section V-C, we have implemented a basic bootstrap filter with 1500 particles, which was sufficient for stable performance. Resampling occurs for a effective sample size below 0.5. More advanced sample strategies could have been considered which would have lead to more stable and accurate filtering, in particular reinitialization [18] would aid our problem. However for the purpose of this qualitative comparison we consider this basic particle filter sufficient.

Because of the significant time-step (multiples of 10 seconds), the computational draw of these algorithms is not considered an important factor as long as the algorithm scales linearly with time. In terms of computation the EKF implementation is, of course, insignificant. A particle filter's computation is linear and is typically a function of the number of particles, in our case off-line testing with 1500 particles was orders of magnitude faster than real-time on a 2.2GHz Core-Duo with 2GB of RAM.

Thirdly, a nonlinear optimization of the entire vehicle trajectory could be carried out. As an example we have implemented a **Nonlinear Least Squares** (NLS) optimizer which iteratively re-optimizes the full path of the AUV when each new measurement is received, using the previous NLS estimate up to that point as the initial condition. Inevitably, the computation required for each successive optimization increases as the number of variables to be optimized grows. To avoid this, one could implement either a windowed estimator (for forgetting factor) using only the most recent portion of the data [10]. Alternatively one could carry our efficient matrix factorization so as to allow optimization of the full path with near-constant computation cost, for example using iSAM [19].

A real-time implementation of the latter has recently been completed and experimental testing is in progress; initial results calculated in post-processing are presented in Section V-C. Given our measurement frequency (less that 1 per 10 seconds), this time constant has been observed to have negligible effect in our proposed application domain.

V. EXPERIMENTAL TESTING

A series of experiments were carried out in the Charles River, adjacent to MIT, to demonstrate the concept of Moving Long Baseline using the Surface Crafts for Oceanographic and Undersea Testing (SCOUT) kayaks designed in MIT and the low-cost Iver2 from OceanServer (see Figure 1). Each of the kayaks was equipped with a WHOI modem, a compass and a GPS sensor while the Iver's basic sensor suite consisted of only a compass and a WHOI modem. The Iver2's only velocity estimate was a *constant* value of 1.028 m/s (2 knots) specified by the mission plan. This value was determined by the manufacturer in advance by calibrating the prop input current to output velocities curve. No feedback was used in executing this velocity.

Each vehicle's on-board computer ran an implementation of the MOOS software platform [28]. Maintaining an accurately synchronized clock is essential for the estimation of inter vehicle ranges; to do so the Iver2 utilized a precisely synchronized timing board developed by Eustice et al. [10] while the SCOUT kayaks used the Pulse-Per-Second (PPS) contained within its received GPS data messages.

A. Distribution of Range Measurements

Previous *proof-of-concept* experiments illustrated that the measured range variance is broadly independent of range itself, however detailed examination of this was not carried out [5]. In this previous work, the modem transducer was directly clamped to the underside of the kayak. In the experiments reported here, the transducer was hung 2-3 meters below the kayak hull; this configuration encounters less noise interference from the kayak motor and less reflections from the water surface.

Figure 5 illustrates the WHOI modem range data plotted versus GPS-derived 'ground truth', as measured in our experimental configuration. Note that because the ground truth distance between the two vehicles was determined using imprecise GPS measurements, it is difficult to precisely estimate the distribution of the range measurements. In the absence of precise ground truth, we estimate the range variance to be between 4–8m.

Finally as the vehicles were moving during the experiment, the accuracy of the ranging function is likely to have been reduced when compared to stationary beacon ranging. However, as the vehicle will be moving we believe that the numbers suggested above are indeed relevant for our scenario.

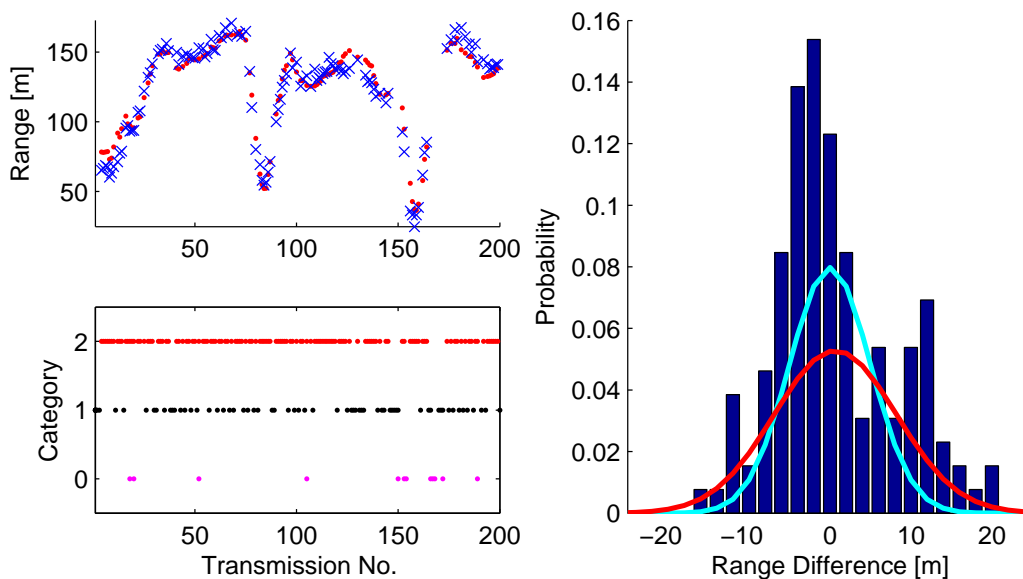


Fig. 5. Analysis of vehicle-to-vehicle range estimates as measured by the WHOI Modem. Upper Left: Comparison of modem range estimate (red dots) and range derived from GPS ‘ground truth’ (blue crosses) for each *fully successful* 10 second transmission period. Lower Left: Illustration of the frequency of successful transmissions. Category 0 represents an entirely failed transmission; Category 1: successful range transmission; Category 2: successful range and packet transmission. Category 2 corresponds to the modem ranges in upper left plot. Right: Histogram of range error (using estimated range versus GPS ‘ground truth’ range), also illustrated is a normal distribution fitted to the data (red, $\bar{r} = 0.66\text{m}$, $\sigma_r = 7.5\text{m}$) and the normal distribution used in the experiments in Section V with (cyan, $\bar{r} = 0\text{m}$, $\sigma_r = 5\text{m}$). This data set corresponds to Experiment 1A.

B. Online Experimental Tests

Experiment 1A: Our initial testing was carried out using a SCOUT kayak designated as the ‘AUV’ (but using real acoustic modem hardware). It completed a survey-type mission while another kayak maintained a zig-zag motion planning pattern behind the ‘AUV’ — taking on the CNA role. The on-board GPS sensor was used to determine the ground truth position. As the vehicles had no direct velocity sensors, the GPS velocity estimate was used simulate forward and starboard velocity measurements. Measurements drawn from the CNA transmissions were used by the ‘AUV’ to reduce its uncertainty. The designated ‘AUV’ carried out 1.5 circuits of a rectangle, covering approximately 1800 meters in total over a period of 37 minutes while the CNA maintained a supporting pattern behind the ‘AUV’, as shown in Figure 6(a).

Note the temporary increase in the error of the position measurement towards the end of the

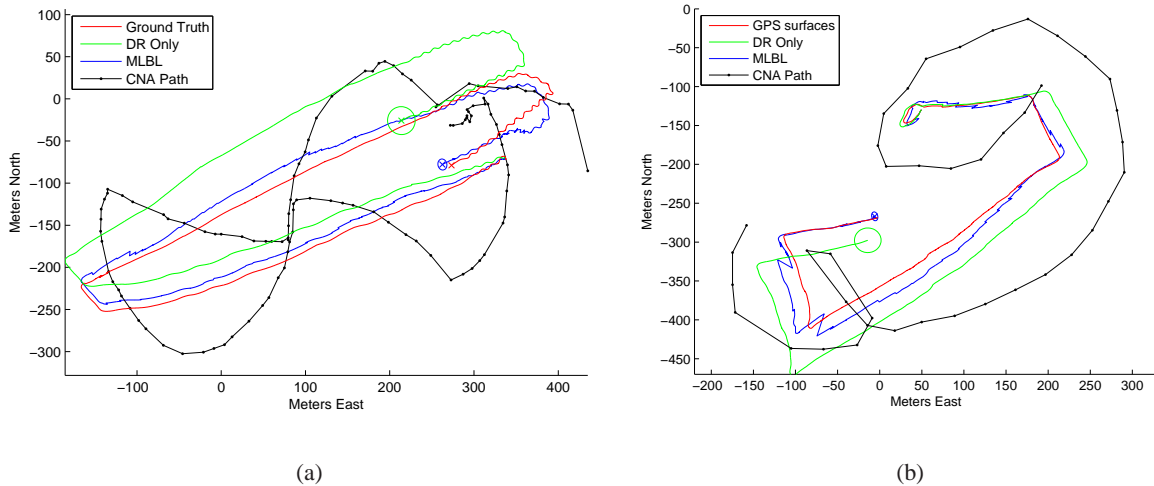


Fig. 6. Paths taken by the simulated AUV and CNA during Experiment 1A and Experiment 1B. CNA measurements were transmitted from the black dots. (a) In Experiment 1A the ‘AUV’ was enabled for one-way ranging while its CNA carried out a zig-zag motion pattern. (b) In Experiment 1B the ‘AUV’ used the fallback of round-trip ranging while its CNA carried out an encircling motion pattern.

experiment. This was caused by two factors: (1) the CNA position estimation was poor, due to only 4 GPS satellites being visible, and (2) the CNA moved on a trajectory that was close, yet parallel, to the AUV, which caused an EKF baseline crossing due to unobservability. While this could have been avoided with the use of a more accurate GPS unit or by forbidding the CNA from taking such a close trajectory, this also provides evidence that the EKF is not the ideal filtering approach.

The following are a number of metrics for this test: mean error 12.5m, mean ‘AUV’ velocity 0.82m/s, mean CNA velocity 1.08m/s. There were 205 transmissions of which 130 were fully successful, 63 resulted in a failed packet transmission but a successful range estimate while 12 resulted in complete transmission failure. The algorithm can be seen to bound the error of the position estimate to approximately 10–15m.

Experiment 1B: Again using one SCOUT kayak in the CNA role and a second simulating the AUV, round-trip ranging (Section II) and an AUV encirclement motion planning behavior was tested. The results are shown in Figure 6(b). The experiment had a duration of 40 minutes, however only 25 minutes of the trajectory is shown for clarity of the figure, to prevent overlap.) The algorithm performed in much the same way as for one-way ranging and the error was

comparable.

However, due to the three step process involved in round trip ranging, the frequency of successful measurements was much lower, leading to navigation instability during measurement blackouts. In particular, in the final third of the experiment, a series of failed transmissions caused the CNA to pass very close to the AUV resulting in baseline ambiguity (which was quickly resolved).

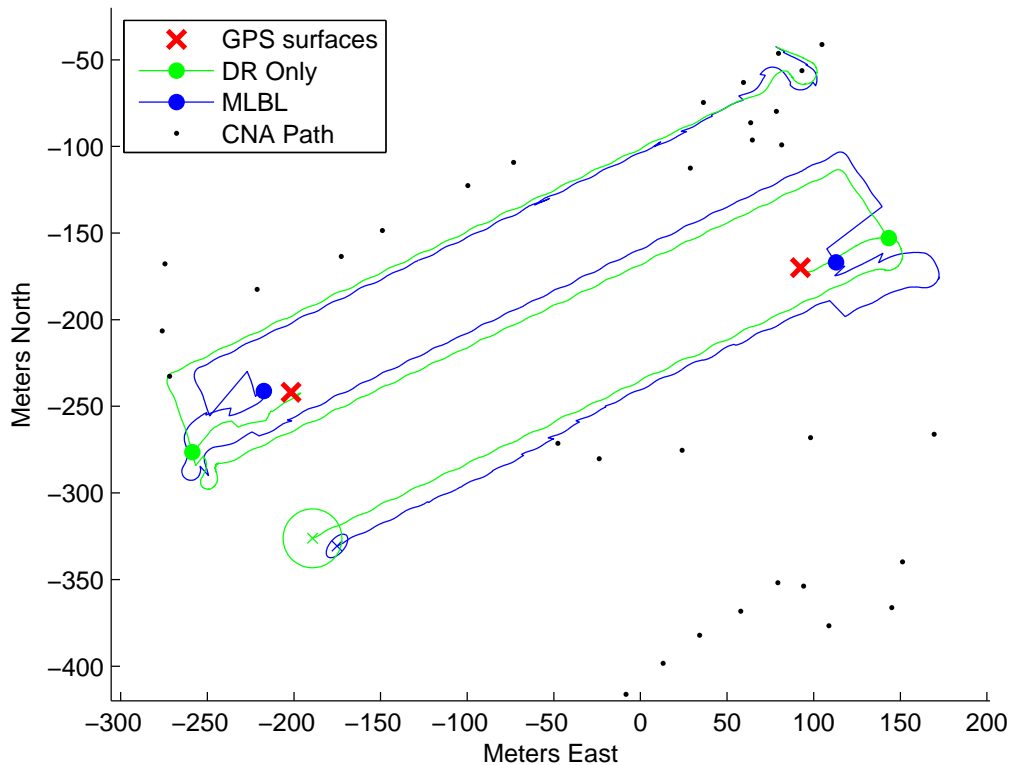


Fig. 7. Paths taken by the OceanServer Iver2 AUV and CNA during Experiment 2. See Section V for more details. CNA measurements were transmitted from the black dots. Locations of the vehicles at the surface positions are shown with markers.

Experiment 2: In a third fully realistic experiment, the OceanServer Iver2 AUV carried out a predefined ‘lawnmower’ pattern running at a depth of 2.4m while the SCOUT kayak supported by transmitting its GPS position to the AUV via the WHOI modem. Operating the MLBL EKF algorithm **entirely online**, the Iver2 transmitted its own position estimates to the CNA. The CNA then used the estimate to plan locations from which to transmit.

Figure 7 illustrates the path taken by the vehicles. The test lasted 28 minutes and in total the Iver2 traveled 2 km. The AUV surfaced twice as a safety precaution. After 9 minutes the AUV first surfaced and received a GPS fix at (-201.6, -242.0) as shown as a red cross, at that time the front seat filter estimated a position of (-258.7,-276.5) while the MLBL filter estimate (-208.9,-238.1) giving an error of 66.7m and 8.3m error respectively (87% lower). When the Iver surfaced for the second time (after 19 minutes), the corresponding errors were 53.7m and 14.1m (74% lower).

For each experiment, the MLBL filter estimates were within a 95% confidence interval when the vehicle came to the surface. After each time the AUV surfaced, it transited from the GPS location back to its planned location on the mission path before diving and continuing the mission.

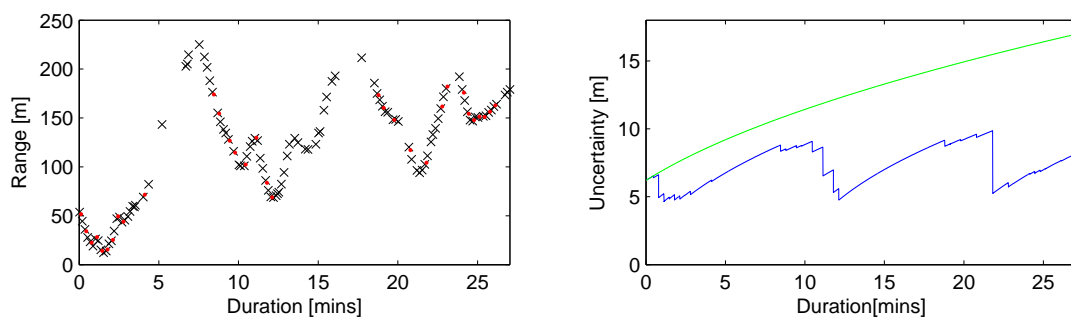


Fig. 8. Results for Experiment 2. Left: Modem range estimates with successful packet transmission (red dots) and modem range estimates but failed packet transmission (black crosses). Right: 95% confidence for the MLBL algorithm (blue) and the dead reckoning along (green). Note the two long portions of the run in which ranges were determined but no packet was successfully transmitted and the resultant growth in position uncertainty.

It should be mentioned that between 4–8 and 12–18 minutes no packets were successfully received by the AUV and as a result no MLBL corrections were possible (See Figure 8). This can be attributed to a number of factors:

- The CNA was positioned behind the AUV and as a result churned water from the AUV propeller is likely to have reduced communication capabilities.
- The AUV and CNA separated to a range of 225m, which is considered long for this experimental river environment. (However note that the maximum range of the WHOI modem in the open ocean is of the order of 2-3 kilometers.)

- The presence of a tourist cruise ship nearby.

In future tests, precautions will be taken to avoid these issues.

C. Comparison of Filtering Algorithms

To perform an experimental between the EKF, particle filter, and nonlinear least squares estimators, we utilized data from an extended 70 minute test in which one CNA localized two kayaks operating as simulated ‘AUVs’. The experiment also illustrated that by using one-way ranging, one surface vehicle can support multiple AUVs using the MLBL approach.

To better approximate realistic operation in a challenging high current environment, in post-processing we add a simulated drift of 0.125 m/s, applied in a south-westerly direction, to the velocity estimates of the simulated AUVs. This simulated drift helps to match the conditions that we would expect to encounter with real low-cost AUVs operating on a long-duration, large scale ocean experiment. The effect of dead-reckoning drift is illustrated in Figure 9 (top) — without outside correction the dead-reckoning of the surrogate AUVs increases substantially with time as the mission progresses. The additional error helps to better illustrate the performance of the different state estimators, and matches the situation that we expect to encounter for our target application of low-cost vehicles operating in the presence of ocean currents.

In the experiment, AUV 1 operated from the beginning of the experiment for the full 70 minutes in the southern portion of the operating area. AUV 2 was added to the northern portion of the operating area after 32 minutes for the remaining 38 minutes of the experiment. The paths that the vehicles took are illustrated in Figure 9. The CNA transmitted its position every 30 seconds, leaving two transmission slots in which the ‘AUVs’ replied with their position estimates (although in this case the CNA did not use this information for adaptive planning). Note that the average velocity of AUV 1 was 1.38 m/s and that of AUV 2 was 0.68 m/s while the CNA velocity was 1.17 m/s. Out of 145 transmissions from the CNA, 113 transmissions (78%) were received at AUV 1 while out of the 79 transmitted. While AUV 2 was operating, 75 transmissions (95%) were received at AUV 2. A passing boat caused significant interference to the acoustic communications between 22 and 25 minutes.

The lower figures show the X and Y paths the two AUVs traveled, as well as the effect that the velocity bias would have had on dead-reckoning during that time. Over the course of the experiment, the dead-reckoning (only) filter estimate continually accrues increasing error, as its

actuator measurements have essentially been biased. In total this results in an error of 550 meters at the end of the experiment. By contrast the MLBL solution (in this case a NLS optimization) can remove the bias by fusing the CNA positions and ranges with the biased dead-reckoning.

Results comparing the post-processed performance of the EKF, particle filter and NLS estimates are presented in Table I. The results presented for the particle filter are averaged over 50 representative runs. Two results are presented for NLS: the error for the final optimized trajectory incorporating all of the measurements and the error for the estimate of the vehicle's location, as estimated on-line. The former is a measure of the quality of the post-processed re-navigated trajectory while the later figure can be compared directly with the EKF and is the position estimate that the vehicle could have acted on so as to navigate. Both were useful in different circumstances.

The error metrics displayed in Table I are the mean error, the mean of the sum of the maximum squared errors, maximum error and the mean absolute error measured relative to the measurements; which are defined as

$$\bar{\epsilon} = \left(\sum_i^N \hat{\epsilon}_i \right) / N \quad (14)$$

$$\bar{\epsilon}_{\text{rms}} = \sqrt{\left(\sum_i^N \epsilon_i^2 \right) / N} \quad (15)$$

$$\epsilon_{\text{max}} = \max(\epsilon_i) \quad \forall i \quad (16)$$

$$\bar{\epsilon}_{\text{meas}} = \left(\sum_i^N | \| X_{A,i} - X_{C,i} \| - z_i | \right) / N \quad (17)$$

respectively. The latter is explicitly what the NLS minimizes. The particle filter position estimate was formed as the simple weighted mean of the particle set, although a kernel estimate would perhaps have been more accurate.

While the experiment was not intended to definitively measure the relative performance of the three algorithms, nonetheless we believe that it allows us to compare the traits of the algorithms. Firstly, we can see that typically the particle filter approach out-performs the EKF. This is to be expected as the particle filter more accurately captures the non-linear range measurement. This is particularly important for the segments of the mission in which poor relative vehicle motion results in poor AUV observability.

Secondly the online NLS algorithm marginally out-performs the particle filter. In the case

Metric	EKF	PF	NLS (online)	NLS (post)	
Mean Error (m)	20.843	15.753	15.127	11.661	AUV 1
Root Mean Squared Error (m)	23.529	17.799	18.647	14.571	
Max. Error (m)	48.994	44.575	55.322	48.352	
Mean Abs. Measurement Error (m)	8.233	5.372	0.213	0.210	
Mean Error (m)	19.484	14.356	14.263	5.710	AUV 2
Root Mean Squared Error (m)	22.177	17.121	16.622	6.259	
Max. Error (m)	44.211	36.383	35.133	11.940	
Mean Abs. Measurement Error (m)	6.613	2.867	0.169	0.154	

TABLE I

Results of the multi-vehicle Cooperative Navigation experiments discussed in Section V for an Extended Kalman Filter, Particle Filter and Nonlinear Least Squares Optimization (with results for online estimates as well subsequently optimized estimates.)

of AUV 2, the online estimate from the NLS algorithm achieves an error of 14.26m while the particle filter is slightly higher with 14.35m error. The performance margin is wider in the case of AUV 1. This can be attributed to the higher mean velocity of that vehicle (1.38m/s vs. 0.68m/s) which causes the particles to be more widely dispersed leading to occasions in which only a small number of particles are located in the vicinity of an estimated range, until the particle filter can recover.

The final post-processed NLS solution gives a mean error of 11.66m and 5.71m respectively, which represents the best estimate. However the final NLS position estimates would not have been available online to the AUV for motion planning.

Finally, we would like to reemphasize that the tracking error values presented in Table I were, for the most part, caused by artificial drift added to the measurements. When the measurements of each sensor are unbiased, each of the three algorithms performs much better (with a mean error of a few meters for the data shown above).

D. AUV Position Initialization

An additional experiment was carried out to demonstrate an initialization of the cooperative navigation system mid-experiment. A sequence of images illustrating this is presented in Figure 10. The AUV had been operating for over an hour and had accumulated significant uncertainty,

as illustrated by the blue ellipse in Step 1. A range and position measurement was then received from the CNA.

Instead of correcting its position using the EKF correction step, which would be unpredictable given the AUV's own uncertainty, the vehicle chose to instead initialize a particle cluster around the range circle circumference (as illustrated in Step 2). Then over the course of successive corrections the particles converged into a unimodal distribution (illustrated successively in Step 3, from black to red to blue).

Finally the particle cluster was replaced with an EKF filter with the same mean and covariance matrix, which then continued to operate as usual for a distance of over 4km (Step 4-5). Note that experiment was carried out in the open ocean, unlike the others, hence the much longer range measurements and distances involved.

VI. CONCLUSIONS AND FUTURE WORK

The concept of a single maneuvering surface vehicle supporting the localization of a fleet of AUVs has been described. The approach requires concurrent operation of vehicle motion planning and filtering algorithms which required consideration of system observability so as to maintain stable and scalable performance. As well as several illustrative simulations, a full online experiment with a single CNA supporting an Iver2 was presented.

The resultant position estimate was shown to be more accurate than the vehicle's own on-board navigation filter. While the AUV experiment illustrated a reduction in error of about 80%, future open water testing will aim to illustrate that this error is in fact bounded by the navigation, ranging and GPS sensors.

Performance comparisons illustrated that both particle filtering and NLS solutions out perform the EKF. An efficient NLS optimization algorithm (based on iSAM [19]) has been implemented; work in progress is evaluating this estimator on a Hydroid REMUS 100 AUV.

Other future work will focus on extending this framework for simultaneous operation on three Iver2 vehicles and eventually towards the scenario in which a set of heterogeneous vehicles are continuously submerged with only a single vehicle occasionally surfacing to access GPS measurements [11].

Finally, the performance of the algorithm is directly determined by the quality and frequency of received measurements. We will consider the optimization of the transmitted messages (and

the re-transmission of failed data) so as to reduce the proportion of useless or partial messages received by the AUV. In this work the CNA motion paths was either a repeating zig-zag or an encirclement pattern. Advanced motion planning of the CNA's path — which takes into account the mission plan of the full AUV fleet — will also be carried out in future.

ACKNOWLEDGMENT

This work was supported by ONR Grant N000140711102 and by the ONR ASAP MURI project led by Princeton University. G. Papadopoulos and N. Patrikalakis was funded by the Singapore National Research Foundation (NRF) through the Singapore-MIT Alliance for Research and Technology (SMART) Center for Environmental Sensing and Modeling (CENSAM).

The authors wish to thank Andrew Patrikalakis, Michael Benjamin, Joseph Curcio and Keja Rowe for their help with the collection of the experimental data and Alexander Bahr and Ryan Eustice for development of the PPS timing boards mentioned in Section II.

REFERENCES

- [1] P.E. An, A.J. Healey, S.M. Smith, and S.E. Dunn. New experimental results on GPS/INS integration using Ocean Voyager II AUV. In *AUV 96*, pages 249–255, June 1996.
- [2] A. Bahr. *Cooperative Localization for Autonomous Underwater Vehicles*. PhD thesis, Massachusetts Institute of Technology, Cambridge, MA, USA, Feb 2009.
- [3] A. Bahr and J. J. Leonard. Minimizing trilateration errors in the presence of noisy landmarks. In *European Conference on Mobile Robots*, 2007.
- [4] A. Bahr and J.J. Leonard. Cooperative Localization for Autonomous Underwater Vehicles. In *Intl. Sym. on Experimental Robotics (ISER)*, Rio de Janeiro, Brasil, Jul 2006.
- [5] J. Curcio, J. J. Leonard, J. Vaganay, A. Patrikalakis, A. Bahr, D. Battle, H. Schmidt, and M. Grund. Experiments in Moving Baseline Navigation using Autonomous Surface Craft. In *Proceedings of the IEEE/MTS OCEANS Conference and Exhibition*, volume 1, pages 730–735, Sep 2005.
- [6] J. Djughash, S. Singh, and P. I. Corke. Further Results with Localization and Mapping using Range from Radio. In *Field and Service Robotics (FSR)*, Jul 2005.
- [7] J. Djughash, S. Singh, and B. P. Grocholsky. Modeling Mobile Robot Motion with Polar Representations. In *IEEE/RSJ Intl. Conf. on Intelligent Robots and Systems (IROS)*, Oct 2009.
- [8] J. Djughash, S. Singh, G. A. Kantor, and W. Zhang. Range-only SLAM for Robots Operating Cooperatively with Sensor Networks. In *IEEE Intl. Conf. on Robotics and Automation (ICRA)*, pages 2078–2084, May 2006.
- [9] A. Doucet, N. de Freitas, and N. Gordon, editors. *Sequential Monte Carlo methods in Practice*. Springer-Verlag, 2000.
- [10] R. M. Eustice, L. L. Whitcomb, H. Singh, and M. Grund. Experimental Results in Synchronous-Clock One-Way-Travel-Time Acoustic Navigation for Autonomous Underwater Vehicles. In *IEEE Intl. Conf. on Robotics and Automation (ICRA)*, pages 4257–4264, Rome, Italy, Apr 2007.

- [11] M. F. Fallon, G. Papadopoulos, and J. J. Leonard. A measurement distribution framework for cooperative navigation using multiple auvs. In *IEEE Intl. Conf. on Robotics and Automation (ICRA)*, pages 4803–4808, May 2010.
- [12] L. Freitag, M. Grund, S. Singh, J. Partan, P. Koski, and K. Ball. The WHOI micro-modem: An acoustic communications and navigation system for multiple platforms. In *Proceedings of the IEEE/MTS OCEANS Conference and Exhibition*, volume 1, pages 1086–1092, Sep 2005.
- [13] A. S. Gadre. *Observability Analysis in Navigation Systems with an Underwater Vehicle Application*. PhD thesis, Virginia Polytechnic Institute and State University, 2007.
- [14] A. S. Gadre and D. J. Stilwell. A complete solution to underwater navigation in the presence of unknown currents based on range measurements from a single location. In *IEEE/RSJ Intl. Conf. on Intelligent Robots and Systems (IROS)*, 2005.
- [15] D. B. Heckman and R. C. Abbott. An acoustic navigation technique. In *IEEE Oceans '73*, pages 591–595, 1973.
- [16] R Hermann and AJ Krener. Nonlinear controllability and observability. *IEEE Transactions on Automatic Control*, pages 728–740, 1977.
- [17] M. Hunt, W. Marquet, D. Moller, K. Peal, W. Smith, and R. Spindel. An acoustic navigation system. Technical Report WHOI-74-6, Woods Hole Oceanographic Institution, 1974.
- [18] M.A. Isard and A. Blake. iCondensation: Unifying low-level and high-level tracking in a stochastic framework. In *Proceedings of the European Conference on Computer Vision*, pages 893–908, 2002.
- [19] M. Kaess, A. Ranganathan, and F. Dellaert. iSAM: Incremental smoothing and mapping. *IEEE Trans. Robotics*, 24(6):1365–1378, Dec 2008.
- [20] C. LaPointe. *A Parallel Hypothesis Method of Autonomous Underwater Vehicle Navigation*. PhD thesis, Massachusetts Institute of Technology, 2009.
- [21] M. B. Larsen. High performance doppler inertial navigation — experimental results. In *IEEE Oceans*, 2000.
- [22] M. B. Larsen. Synthetic long baseline navigation of underwater vehicles. In *IEEE Oceans*, 2000.
- [23] E. Levine, D. Connors, R. Shell, T. Gagliardi, and R. Hanson. Oceanographic mapping with the Navy’s large diameter UUV. *Sea Technology*, pages 49–57, 1995.
- [24] D. K. Maczka, A. S. Gadre, and D. J. Stilwell. Implementation of a cooperative navigation algorithm on a platoon of autonomous underwater vehicles. *Oceans 2007*, pages 1–6, 2007.
- [25] P. H. Milne. *Underwater Acoustic Positioning Systems*. London: E. F. N. Spon, 1983.
- [26] A. I. Mourikis and S. I. Roumeliotis. Performance analysis of multirobot cooperative localization. *IEEE Trans. Robotics*, 22(4):666–681, 2006.
- [27] E.D. Nerurkar, S.I. Roumeliotis, and A. Martinelli. Distributed maximum a posteriori estimation for multi-robot cooperative localization. In *IEEE Intl. Conf. on Robotics and Automation (ICRA)*, pages 1402–1409, May 2009.
- [28] P.M. Newman. MOOS - a mission oriented operating suite. Technical Report OE2003-07, Department of Ocean Engineering, MIT, 2003.
- [29] E. Olson, J.J. Leonard, and S. Teller. Robust range-only beacon localization. *IEEE Journal of Oceanic Engineering*, 31(4):949–958, Oct 2006.
- [30] J. G. Paglia and W. F. Wyman. DARPA’s autonomous minehunting and mapping technologies (AMMT) program: An overview. In *IEEE Oceans*, pages 794–799, Ft. Lauderdale, FL, USA, September 1996.
- [31] P. Rigby, O. Pizarro, and S. B. Williams. Towards geo-referenced auv navigation through fusion of USBL and DVL measurements. In *Proceedings of the IEEE/MTS OCEANS Conference and Exhibition*, Sep 2006.
- [32] J.-J. Slotine and W. Li. *Applied Nonlinear Control*. Prentice-Hall, 1991.

- [33] R. Stokey and T. Austin. Sequential, long baseline navigation for REMUS, an autonomous underwater vehicle. In *SPIE International Symposium on Information systems for Navy divers and autonomous underwater vehicles operating in the surf zone*, volume 3711, pages 3711–25, 1999.
- [34] J. Vaganay, P. Baccou, and B. Jouvencel. Homing by acoustic ranging to a single beacon. In *IEEE Oceans*, pages 1457–1462, 2000.
- [35] J. Vaganay, J. G. Bellingham, and J. J. Leonard. Outlier rejection for autonomous acoustic navigation. In *IEEE Intl. Conf. on Robotics and Automation (ICRA)*, pages 2174–2181, April 1996.
- [36] J. Vaganay, J.J. Leonard, J.A. Curcio, and J.S. Willcox. Experimental validation of the moving long base line navigation concept. In *Autonomous Underwater Vehicles, 2004 IEEE/OES*, pages 59–65, Jun 2004.
- [37] S. E. Webster, R. M. Eustice, C. Murphy, H. Singh, and L. L. Whitcomb. Toward a platform-independent acoustic communications and navigation system for underwater vehicles. In *Proceedings of the IEEE/MTS OCEANS Conference and Exhibition*, Biloxi, MS, 2009.
- [38] S. E. Webster, R. M. Eustice, H. Singh, and L. L. Whitcomb. Preliminary deep water results in single-beacon one-way-travel-time acoustic navigation for underwater vehicles. In *IEEE/RSJ Intl. Conf. on Intelligent Robots and Systems (IROS)*, 2009.
- [39] L. Whitcomb, D. Yoerger, H. Singh, and D. Mindell. Towards precision robotic maneuvering, survey, and manipulation in unstructured undersea environments. In *Proc. of the Intl. Symp. of Robotics Research (ISRR)*, volume 8, pages 45–54, 1998.
- [40] D. Yoerger, M. Jakuba, A. Bradley, and B. Bingham. Techniques for deep sea near bottom survey using an autonomous underwater vehicle. *Robotics Research*, pages 416–429, 2007.

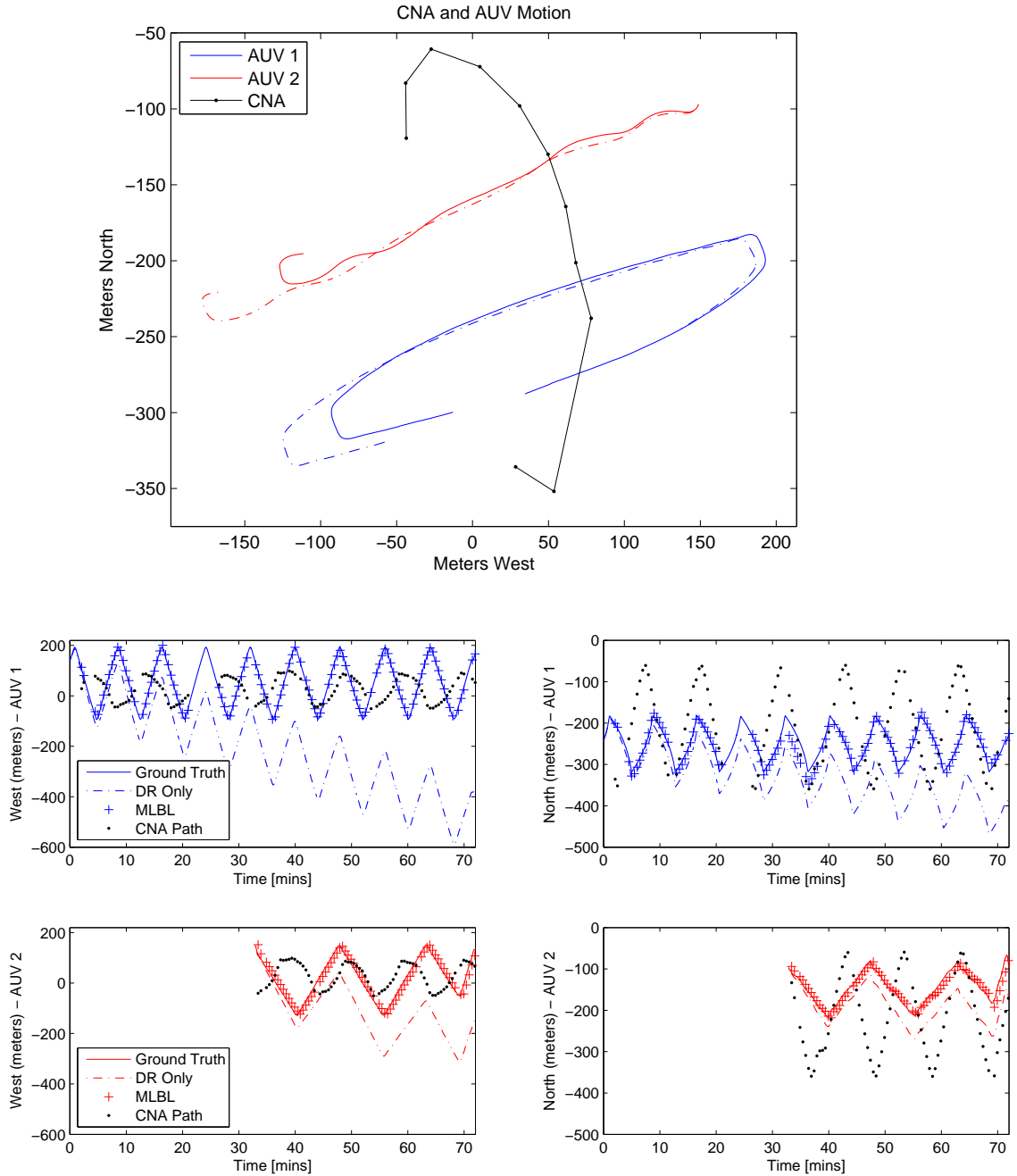


Fig. 9. Motion of the 3 vehicles used in the experiment in Section V-C. Upper: An overhead view of 7 minutes of the simulated AUV motion (which was repeated for the duration). Illustrated is the ground truth (solid lines) and the current-biased dead-reckoning (dashed lines) as well as the locations from which the CNA transmitted (black dots). AUV 1 and the CNA moved anti-clockwise while AUV 2 moved clockwise. Lower: the X and Y motion of the simulated AUVs. The upper plots correspond to AUV 1 and the lower plots to AUV 2. The ground truth during the experiment (solid lines), the biased dead-reckoning (dashed lines), the CNA transmission locations (dots) and the MLBL solution formed by fusing the dead-reckoning and the CNA positions and ranges (crosses) are illustrated. Note that AUV 2 was introduced to the mission after 32 minutes.

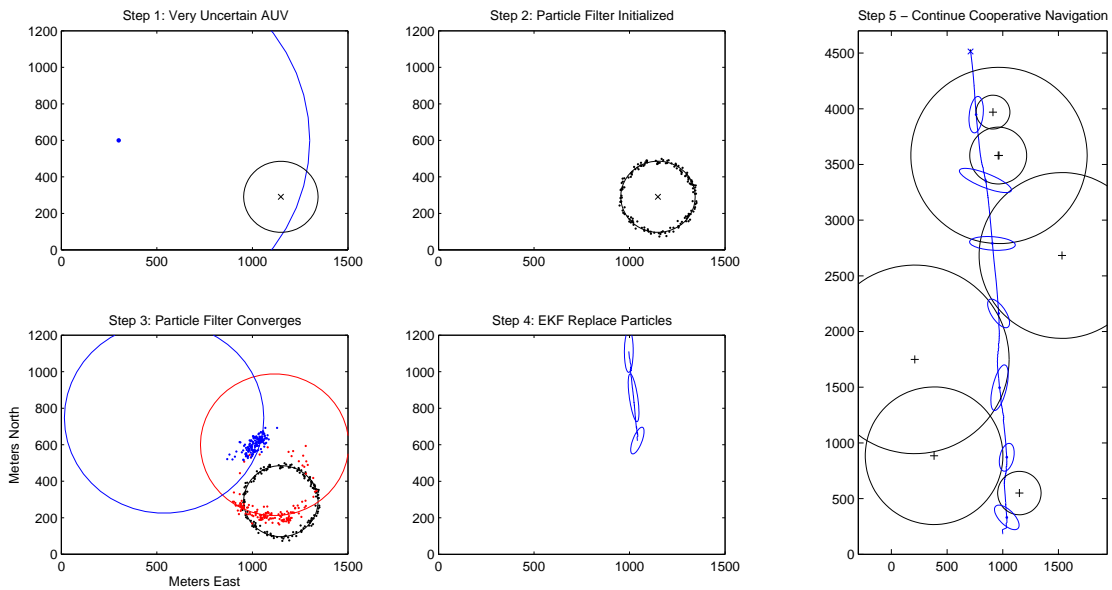


Fig. 10. Re-initialization of the AUV position estimate using a particle filter. An uncertain AUV position estimate (blue, Step 1) is replaced by a particle cluster scattered around a range and position measurement (black, Step 2). Successive correction steps cluster the particles in a unimodal cluster (black-red-blue, Step 3) until finally the EKF recommences using the mean and covariance of particle cluster as its starting point which continues to track (Step 4-5). Only a portion of the particles and the correction steps are illustrated. See Section V-D for more details.